Power Stabilization Based on Efficiency Optimization for WPT Systems With Single Relay by Frequency Configuration and Distribution Design of Receivers

Wei Wang, Xueliang Huang, *Member, IEEE*, Jinpeng Guo, Han Liu, Changxin Yan, and Linlin Tan

***Abstract*—The operation of wireless power transfer systems (WPT) with a single relay, which could charge one or multiple receivers simultaneously, is investigated. Besides, a new method for ensuring the optimized transfer efficiency and the output power by configuring the operating frequency is presented, even when the coupling coefficients between all the coils are very small. An issue of concern is that the couplings between receivers cannot be ignored due to limited operating space, which adds to the complexity of both the system design and the control method. The contribution of the research presented here is to propose an optimized strategy which can charge each receiver with identical power and simplify the coupling complexity thereof. Specifically, the efficiencies and outputs of the introduced WPT systems are discussed. In addition, the distribution design according to different numbers of receivers is proposed to guarantee that both the system operating frequency and the output power remain stable. The theoretical analysis is confirmed by both simulation and experimental results.**

***Index Terms*—Distribution design, efficiency optimization, frequency configuration, power stabilization, wireless power transfer.**

I. Introduction

WIRELESS power transfer (WPT) is now becoming more and more important as an alternative technology for domestic and industrial applications, because of the user-friendly nature of wireless connection. Comparatively, the traditional charging with cables presents several disadvantages in particular fields such as the deep sea, coal mining, and chemical industries. Specifically, problems such as sparks and the difficulty of laying and maintaining power lines are inevitable. As a result, the WPT has been applied in many areas. Many studies have been performed on wireless battery charging for intelligent devices [1]–[3]. Apart from this, proponents of implantable medical applications have shown a great desire for technology capable of relieving the pain resulting from the replacement of batteries [4]–[6]. Attempts have been made to enable a cord-free desk by embedding primary coils under the desk so that the desktop electronic devices can be charged more conveniently [7], [8]. The massive application of WPT technology has in turn led to the formation of the Wireless Power Consortium and its launch of the first wireless power standard "Qi" [9]. With the development of high-frequency electrical electronic devices, WPT technology also exhibits potential application in the large power field including the wireless charging for electric vehicles and the dynamic power supply necessary for transportation applications [10]–[13]. This has become a research focus for WPT.

The WPT systems with two resonant coils compensated by series or parallel capacitors are deeply analyzed. The equivalent circuit model has been widely used to analyze the transmission performance of the traditional WPT system [14], [15]. However, one significant bottleneck in the technology is its sensitivity to distance so that WPT is widely adopted in close charging for low-power instruments. On the contrary, the demand for long-distance wireless charging should be satisfied to meet public demands. An improved method involves the use of relay coils (RCs) as coupling-enhanced devices, which are connected to the resonant circuits, to improve the coupling coefficients between the coils and relieve the drastic decrease of the reflected impedance when the transfer distance increases [16]–[18]. In addition, the RCs can also improve the efficiency performance. It has been pointed out in [19] and [20] that a three-coil WPT system could be more energy efficient than a two-coil counterpart, with up to 38.4% improvement. Consequently, the excellent performance, as well as the convenient design of a three-coil WPT, has attracted much attention, which is also the foundation of this paper.

Inclusive WPT systems have been considered as offering guidance of their industrial development due to their advantages of applicability and feasibility. Examples of such applications include the wireless charging systems for office desks and coffee tables, which may be equipped with the RCs under the table surfaces and the excitation coil under the floor. As for each electronic device which meets the Qi criteria, the power can be received with the embedded receiving coil regardless of the number of variations therein. Theoretically, the inclusive WPT systems involve investigations of charging for multiple receivers. Similarly, the efficiency optimization and the power stability are still the ultimate goals of a multiload WPT system. Elsewhere, Nguyen *et al.* [21] used a metamaterial

Manuscript received May 17, 2016; revised July 31, 2016 and September 11, 2016; accepted October 31, 2016. Date of publication November 8, 2016; date of current version April 24, 2017. This work was supported in part by the National Natural Science Youth Foundation of China under Grant 51507032, and in part by the Natural Science Youth Foundation of Jiangsu Province under Grant BK20150617. Recommended for publication by Associate Editor O. Lucia.

The authors are with the Department of Electrical Engineering, The Southeast University, Nanjing 210096, China (e-mail: wangw_seu@ 163.com; gjp1992@sina.com; gjp1992@sina.com; liuhan199305@163.com; sireagle@foxmail.com; tanlinlin@seu.edu.cn).

Color versions of one or more of the figures in this paper are available online at http://ieeexplore.ieee.org.

Digital Object Identifier 10.1109/TPEL.2016.2626498

array near the load coil to concentrate the magnetic field and enhance the transfer efficiency of multiloads systems. Others, authors in [22]–[24] introduced one of the most commonly adopted methods of improving the transmission efficiency, the impedance matching technology to track the optimal load by circuit transformation. Authors in [25] and [26], on the other hand, proposed the tracking of the optimal frequency to achieve the maximum efficiency but only a WPT system without RCs was taken into account. In addition to the efficiency performance, the stable output power should also be considered especially in circumstances where the number of charging devices changed frequently. Authors in [27] and [28] analyzed the power division ratio of loads with different impedances. It is noted that most investigations have been carried out on the power division with impedance conversion; in practical applications, the key point is how to enable stable charging power of each load when the number of loads varies, which may result in fluctuation of the charging power.

Here, it is proposed that the resonant and operating frequencies of a system with a single RC and a single load, and that with a single RC and multiple loads, should be configured to optimize the transfer efficiency and maximize the output power. In case of weak coupling, the efficiency can be improved by 24% and the output power is increased from 2.9 to 31.6 W with the frequency configuration used. This paper also introduces a novel distribution design of receivers to ensure identical receiving power. On this basis, an optimization strategy to keep stable operating frequency and charging power is proposed when the number of loads varies. Experimental results show that the power fluctuation of each receiver can be kept to within ± 0.3 W. The theory can be applied to the low-power applications such as a planar wireless charging desk with an extended air gap and long legs.

II. Analysis of a Single Relay and Receiver

The use of a RC can undoubtedly increase the transfer distance and improve the system performance in terms of efficiency and output power. The series compensated resonators are used as an example in this paper to investigate the influence of operating frequency on the coupling ability. An equivalent circuit model of the system is shown in Fig. 1, including the driving source U_s working at frequency ω, the transmitting coil (TC), the RC and the receiving coil (R_1C) working at frequencies ω_{TX}, ω_r, and ω_{RX}, respectively. The self-resonant frequencies satisfy: $\omega_{\mathrm{TX}} = 1/\sqrt{L_tC_t}$, $\omega_r = 1/\sqrt{L_rC_r}$, and $\omega_{\mathrm{RX}} = 1/\sqrt{L_1C_1}$.

As shown in Fig. 1, R_s and R_L denote the source resistance and the load resistance, respectively; R_t, C_t, and L_t are the resistance, the resonant capacitance, and the inductance of the TC; R_r, C_r, and L_r are the resistance, the resonant capacitance, and the inductance of the RC; R_1, C_1, and L_1 represent the resistance, the resonant capacitance, and the inductance of the $\mathrm{R_1C}$; the coupling coefficient between the TC and the RC, and that between the RC and the $\mathrm{R_1C}$, are expressed as k_{tr} and k_{r1}, respectively.

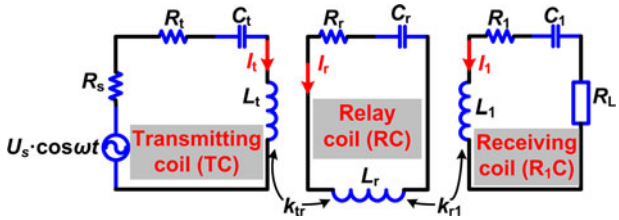

Fig. 1. Circuit topology of a WPT system with a single RC.

A. Frequency Configuration to Maximize the Efficiency

As for the three-coil WPT system shown in Fig. 1, the system transfer efficiency can be expressed by the ratio of load consuming power and the source exporting power

$$\eta = \frac{|\mathbf{I_1}|^2 R_L}{|\mathbf{I_t}|^2 R_{st} + |\mathbf{I_r}|^2 R_r |\mathbf{I_1}|^2 R_{1L}} = \frac{R_L}{\left|\frac{\mathbf{I_t}}{\mathbf{I_1}}\right|^2 R_{\mathrm{st}} + \left|\frac{\mathbf{I_r}}{\mathbf{I_1}}\right|^2 R_r + R_{1L}} \tag{1}$$

where $|\mathbf{I_t}|$,$|\mathbf{I_r}|$, and $|\mathbf{I_1}|$ represent the model values of the current in each coil. R_{st} and R_{1L} are used to represent the resistance of the TC and the R_1C loop, respectively, which can be calculated by $R_{\mathrm{st}} = R_s + R_t$, $R_{1L} = R_1 + R_L$. From (1), it can be inferred that the system transfer efficiency can be maximized by minimizing $|\mathbf{I_t}/\mathbf{I_1}|$ and $|\mathbf{I_r}/\mathbf{I_1}|$ at the same time. The specific expressions of $|\mathbf{I_t}/\mathbf{I_1}|$ and $|\mathbf{I_r}/\mathbf{I_1}|$ can be deduced by applying Kirchhoff's voltage law (KVL)

$$\mathbf{I_t}\left(1 - \frac{{\omega_{\mathrm{TX}}}^2}{\omega^2} - j\frac{R_{\mathrm{st}}}{\omega L_t}\right) + \mathbf{I_r} k_{\mathrm{tr}}\sqrt{\frac{L_r}{L_t}} = -j\frac{U_s}{\omega L_t} \tag{2.a}$$

$$\mathbf{I_t} k_{\mathrm{tr}}\sqrt{\frac{L_t}{L_r}} + \mathbf{I_r}\left(1 - \frac{{\omega_r}^2}{\omega^2} - j\frac{R_r}{\omega L_r}\right) + \mathbf{I_1} k_{r1}\sqrt{\frac{L_1}{L_r}} = 0 \tag{2.b}$$

$$\mathbf{I_r} k_{r1}\sqrt{\frac{L_r}{L_1}} + \mathbf{I_1}\left(1 - \frac{{\omega_{\mathrm{RX}}}^2}{\omega^2} - j\frac{R_{1L}}{\omega L_1}\right) = 0 \tag{2.c}$$

where $k_{\mathrm{tr}} = L_{\mathrm{tr}}/\sqrt{L_t \cdot L_r}$, and $k_{r1} = L_{r1}/\sqrt{L_r \cdot L_1}$. L_{tr} and L_{r1} denote the mutual inductance between the TC and the RC, and that between the RC and the R_1C, respectively. Given the coupling between the TC and the R_1C is small enough to be ne-

$$\left|\frac{\mathbf{I_r}}{\mathbf{I_1}}\right| = \left|\frac{1 - {\omega_{\mathrm{RX}}}^2/\omega^2 - jR_{1L}/\omega L_1}{k_{r1}\sqrt{L_r/L_1}}\right| \tag{3.a}$$

$$\left|\frac{\mathbf{I_t}}{\mathbf{I_1}}\right| = \left|\frac{(1 - {\omega_{\mathrm{RX}}}^2/\omega^2 - jR_{1L}/\omega L_1)\cdot(1 - {\omega_r}^2/\omega^2 - jR_r/\omega L_r) - {k_{r1}}^2}{k_{\mathrm{tr}} k_{r1}\sqrt{L_t/L_1}}\right| \tag{3.b}$$

glected, the following analysis will ignore the weak coupling and exert no effect on the correctness of the theoretical mechanism.

It can be calculated from (2.a)–(2.c) that Equation (3Za)-(3Zb) as shown at the bottom of the previous page.

If $|\frac{\mathbf{I_t}}{\mathbf{I_1}}|_{\min}$ and $|\frac{\mathbf{I_r}}{\mathbf{I_1}}|_{\min}$ can be guaranteed, then the system transfer efficiency can achieve its maximum value. In addition, the quality factor of each resonant coil needs to reach a high level. When all other parameters are constant, the condition to maximize the transfer efficiency, according to (3.a) and (3.b), can be expressed by

$$\begin{cases} \omega = \dfrac{\sqrt{2}L_1{\omega_{\mathrm{RX}}}^2}{\sqrt{2{\omega_{\mathrm{RX}}}^2{L_1}^2 - {R_{1L}}^2}} \cong \omega_{\mathrm{RX}} \\ \omega = \omega_r . \end{cases} \tag{4}$$

The approximation in (4) holds for $2\omega_{\mathrm{RX}}^2 L_1^2 >> R_{1L}^2$, which is valid when the WPT system is powering a load with small resistance. It proves that the maximum efficiency can be ensured even when the coupling between coils is very weak.

B. Frequency Configuration to Maximize the Output Power

In addition to the efficiency performance, a typical design objective is to increase the output power as much as possible. The receiving power of the load is

$$P_L = |\mathbf{I}_1|^2 \cdot R_L . \tag{5}$$

In circumstances where the load resistance is fixed, the only factor determining the output power is the model value of $\mathbf{I_1}$. Under the condition needed to achieve the maximum efficiency, the load current $\mathbf{I_1}$ is described by (6) shown at the bottom of the page.

$\mathbf{I_1}$ can be maximized by setting the imaginary part of (6) to zero, namely it should conform to $\omega_{\mathrm{TX}} = \omega_r$. As a result, to make the most of a three-coil WPT system with a single load, the system operating frequency and the resonant frequencies of each coil ought to satisfy

$$\omega = \omega_{\mathrm{TX}} = \omega_r \cong \omega_{\mathrm{RX}} . \tag{7}$$

The specific relationship between the system performance and the frequency is shown in Fig. 2. To make the annotation in following figures accurate, the time-domain frequency is used to replace the angular frequency.

As indicated by Fig. 2(a), the system transfer efficiency is closely related to the operating frequency when the self-resonant parameters of each coil remain unchanged. The specific parameters of the proposed WPT system in Fig. 2(a) are as follows: the inductances of the TC and the RC are both 176 μH; the coupling coefficient between the TC and the RC is 0.03; L_1 is 20 μH, and the coupling coefficient between the R_1C and the RC is 0.016; R_{st}, R_r, and R_{1L} are 1.1, 0.1, and 2.03 Ω, respectively. In addition, the original resonant frequencies of the TC and the R_1C are 480 and 520 kHz. When $\omega_r \neq \omega_{\mathrm{RX}}$ and the system operating frequency is set between ω_r and ω_{RX}, the system transfer efficiency can reach its maximum value, but it is still far from the ideal results as demanded. Only when $\omega = \omega_r = \omega_{\mathrm{RX}}$ can it be ensured that the maximum system transfer efficiency under all conditions is reached, which is greater than any efficiency value for $\omega_r \neq \omega_{\mathrm{RX}}$. It is also noted that there is a deviation of 7 kHz between ω and ω_{RX}, which is caused by the low quality factor Q of the R_1C loop. Similarly, according to Fig. 2(b), the excitation voltage (U_s) is 20 V, and $\omega = \omega_r = \omega_{\mathrm{RX}} = 480$, 500, and 530 kHz, respectively. Besides, the other parameters are the same as those in Fig. 2(a). On the premise of the maximum efficiency, the output power is determined by the self-resonant frequency ω_{TX} of the TC loop. In detail, the output power can be maximized only when ω_{TX} is equal to the operating frequency.

III. Analysis of Multiple Coupled Receivers

As for the three-coil WPT system with multiple loads, it is necessary to provide enough power for multiple loads simultaneously. Typical features of the three-coil WPT system with multiple loads are that receiving coils are restricted to a limited space and the transfer distance is relatively long. In this sense, the coupling between the receiver and the transmitter is weak. As a result, it is of great significance to ensure the system performance by optimizing the operating frequency and the self-resonant frequency of each coil loop. On the basis of the determined frequency, the effect of different numbers of loads on the system transfer efficiency and the output power will be investigated in the following analysis to maintain loads working stably.

A. Distribution Optimization of Receiving Coils

The three-coil WPT system is always used to supply low-power devices such as sensor nodes, mobile telephones, etc. Although not too much power (in total) is needed, the power distribution is required to be uniform (as far as possible) especially when the number of loads changes.

To illustrate the distribution optimization of receiving coils, the helical coils connected with the same load are used here. It can be inferred that the receiving power of each receiver is determined by the coupling coefficient between any receiver (denoted by *i*) and the RC, and the sum of coupling coefficients between each receiver and the other receivers. To ensure that a uniform power was received by each receiver, the constraints are shown in

$$\begin{cases} k_{\mathrm{ri}} = \Gamma_1 \\ \sum_{j'=1}^{n} k_{\mathrm{ij'}} = \Gamma_2 \end{cases} \quad (i \in [1,n], j' \neq i, \Gamma_1 \in \mathbb{R}, \Gamma_2 \in \mathbb{R}, n \in \mathbb{N}) \tag{8}$$

where Γ_1 and Γ_2 represent any real numbers, and *n* denotes the number of receiving coils.

$$\mathbf{I_1} = -\frac{{\omega_r}^2 L_r L_1 k_{\mathrm{tr}} k_{r1}\sqrt{L_t/L_1}\cdot U_s}{{\omega_r}^2 L_r L_1 {k_{\mathrm{tr}}}^2 R_{1L} L_t/L_1 + R_{\mathrm{st}} R_r R_{1L} + {k_{r1}}^2 {\omega_r}^2 L_r L_1 R_{\mathrm{st}} + j\omega_r L_t (1-{\omega_{\mathrm{TX}}}^2/{\omega_r}^2)(R_r R_{1L} + {\omega_r}^2 L_r L_1 {k_{r1}}^2)} \tag{6}$$

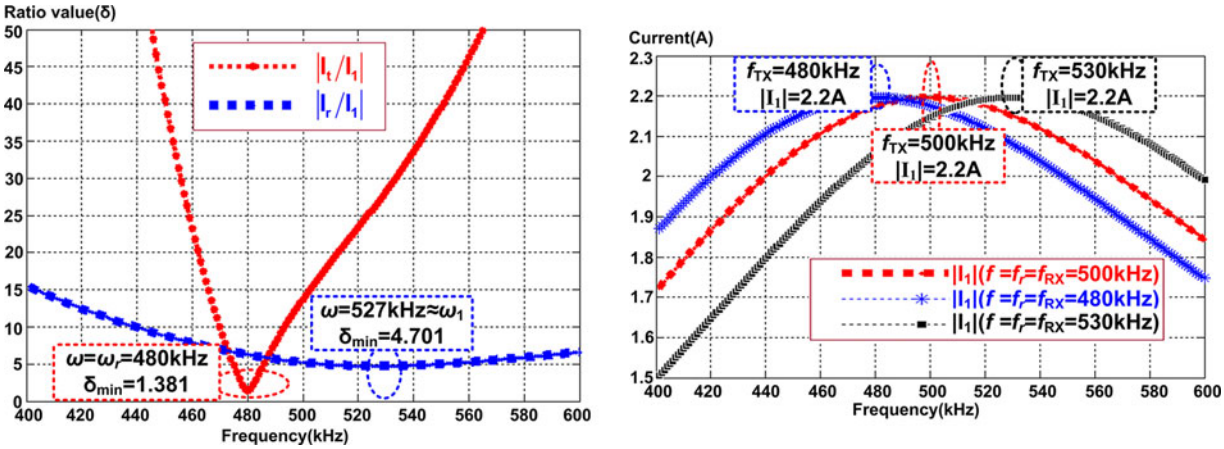

Fig. 2. Relationship between system performance and frequency. (a) RMS of current ratios of $\mathbf{I_t}$ to $\mathbf{I_1}$ and $\mathbf{I_r}$ to $\mathbf{I_1}$. (b) RMS of load current ($|\mathbf{I_1}|$) changes with the operating frequency when the resonant frequencies of TC (ω_{TX}) are 480, 500, and 530 kHz, respectively.

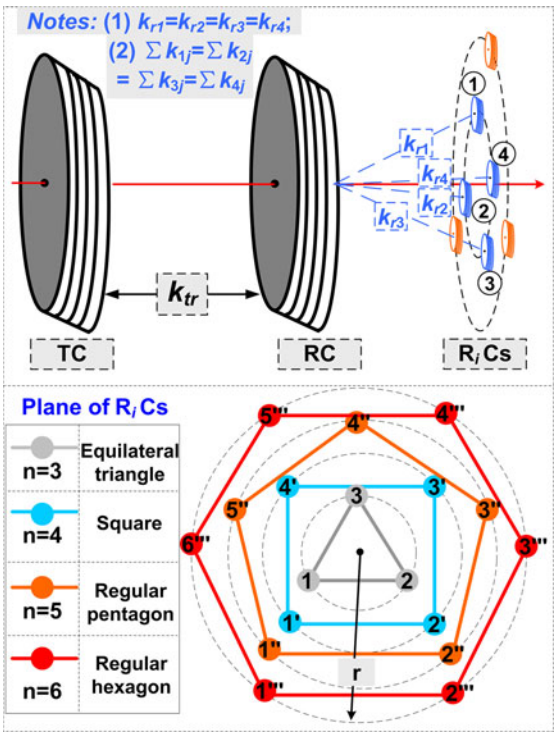

Fig. 3. Distributions of the varied numbers of loads. Only the distributions of the three to six receiving coils are given in this paper as examples.

The specific distribution of the three-coil system is shown in Fig. 3. Considering the applications requiring supply-platforms such as charging for mobile telephones [29], all receiving coils are placed on a surface and are parallel with the TC and RC.

Each receiving coil can receive identical power as long as the receivers are placed as shown in Fig. 3. The centers of the TC and the RC are coaxial with that of the loads, which are distributed in regular polygons; however, an unresolved problem is that the charging power of each load may also fluctuate when the number of receiving coils changes. As a result, the equivalent model of a multiload system must therefore be investigated.

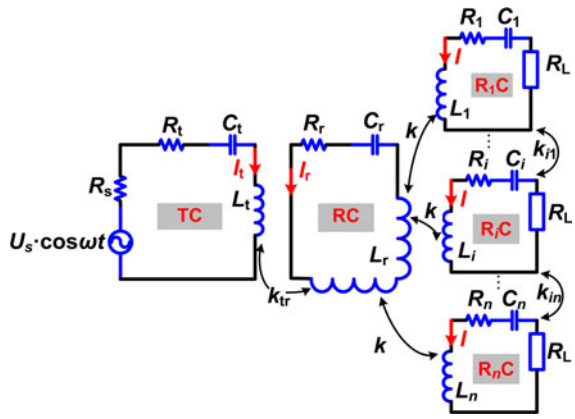

Fig. 4. WPT from single TC and RC to multiple receivers.

B. Equivalent Circuit Analysis of a System With Multiple Loads

Equivalent circuit model of a WPT system with a single relay and multiple loads is complicated. With the distribution method introduced in Fig. 3, the analysis can be simplified to ensure theoretical correctness at the same time. A typical equivalent circuit model of the three-coil WPT system with multiple loads is shown in Fig. 4.

In Fig. 4, the RC is coupled with each receiving coil with a coupling coefficient of k. The current in each receiving coil is $\mathbf{I}$, and the coupling coefficient between one receiving coil and another is k'_{ij}. As the parameters of each receiving loop are the same, the original resonant frequency of each receiving loop is represented as ω_{RX}. And the current in each receiving coil is $\mathbf{I}$. Based on the KVL

$$\mathbf{I_t}\left(1-\frac{{\omega_{\mathrm{TX}}}^2}{\omega^2}-j\frac{R_{\mathrm{st}}}{\omega L_t}\right)+\mathbf{I_r}k_{\mathrm{tr}}\sqrt{\frac{L_r}{L_t}}=-j\frac{U_s}{\omega L_t} \tag{9.a}$$

$$\mathbf{I_t}k_{\mathrm{tr}}\sqrt{\frac{L_t}{L_r}}+\mathbf{I_r}\left(1-\frac{{\omega_r}^2}{\omega^2}-j\frac{R_r}{\omega L_r}\right)+n\mathbf{I}\cdot k\cdot\sqrt{\frac{L_i}{L_r}}=0 \tag{9.b}$$

$$\mathbf{I_r}k\cdot\sqrt{\frac{L_r}{L_i}}+\mathbf{I}\cdot\left(1-\frac{{\omega_{\rm RX}}^2}{\omega^2}-j\frac{R_{iL}}{\omega L_i}+\sum_{j'=1}^{n}k_{ij'}\right)=0 \tag{9.c}$$

where $k_{\rm tr}=L_{\rm tr}/\sqrt{L_t\cdot L_r}$, and $k=L_{\rm ri}/\sqrt{L_r\cdot L_i}$. As a result, the overall transfer efficiency can be described by

$$\eta=\frac{nR_L}{\left|\frac{\mathbf{I_t}}{\mathbf{I}}\right|^2R_{\rm st}+\left|\frac{\mathbf{I_r}}{\mathbf{I}}\right|^2R_r+nR_{iL}}. \tag{10}$$

In (10), R_{iL} is the loop resistance of each receiving loop. By solving (9.a)–(9.c), it can be deduced (11a)–(11b) as shown at the bottom of the page.

As obviously seen from (10), the decrease of $|\mathbf{I_t}/\mathbf{I}|^2$ and $|\mathbf{I_r}/\mathbf{I}|^2$ will contribute to the increase of system transfer efficiency. Efficiency can be maximized when $|\mathbf{I_t}/\mathbf{I}|^2$ and $|\mathbf{I_r}/\mathbf{I}|^2$ are minimized at the same time. According to (11.a), the corresponding condition of the minimal $|\mathbf{I_t}/\mathbf{I}|^2$ and the result of $\mathrm{MIN}(|\mathbf{I_t}/\mathbf{I}|^2)$ are

$$\begin{cases}\omega=\omega_r\\ \left|\mathbf{I_t}/\mathbf{I}\right|^2=\dfrac{n^2k^2L_i}{{k_{\rm tr}}^2L_t}.\end{cases} \tag{12.a}$$

Similarly, the corresponding condition of the minimal $|\mathbf{I_r}/\mathbf{I}|^2$ and the result of $\mathrm{MIN}(|\mathbf{I_r}/\mathbf{I}|^2)$ are

$$\begin{cases}\omega=\dfrac{\sqrt{2}L_i{\omega_{\rm RX}}^2}{\sqrt{2{\omega_i}^2{L_i}^2\left(1+\sum_{j'=1}^{n}k_{ij'}\right)-{R_{iL}}^2}}\\ \quad\cong\dfrac{\omega_{\rm RX}}{\sqrt{1+1+\sum_{j'=1}^{n}k_{ij'}}}\\ \left|\mathbf{I_r}/\mathbf{I}\right|^2\cong\dfrac{1}{{Q_i}^2}\dfrac{L_i}{k^2L_r}\left(1+\sum_{j'=1}^{n}k_{ij'}\right)\end{cases} \tag{12.b}$$

where Q_i is the quality factor of each receiving coil loop and is $\omega_{\rm RX}L_i/R_{iL}$. The approximation holds for $2{Q_i}^2\gg 1/(1+\sum_{j'=1}^{n}k_{ij'})$. From the previous analysis, it can be concluded that the maximum transfer efficiency when other parameters are fixed is

$$\omega=\omega_r=\frac{\omega_{\rm RX}}{\sqrt{1+\sum_{j'=1}^{n}k_{ij'}}}. \tag{13}$$

In other words, $\omega_{\rm RX}=\omega_r\cdot\sqrt{1+\sum_{j'=1}^{n}k_{ij'}}$. Then, the maximum transfer efficiency is expressed by (14) shown at the bottom of the page.

On the premise of the maximum transfer efficiency, it is also required to provide enough power for the required loads. Assuming that the power demand of a load is $P_{\min}$ and the receiving power is P_L, $P_L\geq P_{\min}$ shall be satisfied. For a load with fixed resistance, P_L is proportional to $|\mathbf{I}|^2$ which is calculated by (15) as shown at the bottom of the next page, where Q_r is the quality factor of the RC loop and is $\omega L_r/R_r$. Once other system parameters are determined, the model value of $\mathbf{I}$ can be maximized when $\mathrm{Im}(\mathbf{I})=0$. From (15), it can be deduced that the frequency should conform to

$$\omega_{\rm TX}=\omega_r. \tag{16}$$

The coupling coefficient *k* is also very small, so a small value of $1/Q_rQ_i$ caused by coils with a high-quality factor cannot be ignored. According to (16), the receiving power of each receiver can be expressed by

$$\begin{cases}|\mathbf{I}|=\dfrac{U_sk_{\rm tr}k\cdot\sqrt{L_t/L_i}}{\left|(nk^2-1/Q_rQ_i)R_{\rm st}-k_{\rm tr}\sqrt{L_t/L_r}R_{iL}L_t/L_i\right|}\\ P_L=|\mathbf{I}|^2R_L.\end{cases} \tag{17}$$

In conclusion, to achieve the maximum output power on the basis of proving the maximum transfer efficiency, the operating frequencies should satisfy

$$\omega=\omega_{\rm TX}=\omega_r\cong\frac{\omega_{\rm RX}}{\sqrt{1+\sum_{j'=1}^{n}k_{ij'}}}. \tag{18}$$

Generally speaking, the operating frequency, and the self-resonant frequencies of both the TC and the RC should be set to identical values regardless of the number of receiving coils. In addition, the self-resonant frequency of the receiving coils should be set in accordance with the number of receiving coils. To power a single load, the self-resonant frequency of the receiving coil should be the same as the operating frequency. To power multiple loads, the original resonant frequency of the receiving loop should be adjusted according to (18), which is determined mainly by the sum of coupling coefficients between one receiving coil and others.

$$\left|\frac{\mathbf{I_t}}{\mathbf{I}}\right|=\left|\frac{nk^2-(1-{\omega_r}^2/\omega^2)\left[\left(1-{\omega_{\rm RX}}^2/\omega^2+1+\sum_{j'=1}^{n}k_{ij'}\right)+jR_{iL}/\omega L_i\right]}{k_{\rm tr}k\cdot\sqrt{L_t/L_i}}\right| \tag{11.a}$$

$$\left|\frac{\mathbf{I_r}}{\mathbf{I}}\right|=\left|\frac{1-{\omega_{\rm RX}}^2/\omega^2+1+\sum_{j'=1}^{n}k_{ij'}-jR_{iL}\Big/\omega L_i}{k\sqrt{L_r/L_i}}\right| \tag{11.b}$$

$$\eta=\frac{nR_L}{n^2k^2L_iR_{\rm st}\Big/\left({k_{\rm tr}}^2L_t\right)+\left(1+\sum_{j'=1}^{n}k_{ij'}\right)R_rL_i\Big/\left(k^2{Q_i}^2L_r\right)+nR_{iL}} \tag{14}$$

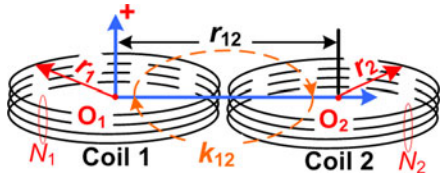

Fig. 5. Coupling coefficient calculation setup for paired spiral coils.

IV. Methods of Design Optimization

A. Stabilization of Optimized Frequency

Based on the said analysis, it can be seen that the optimal operating frequency varies according to the number of loads, as illustrated by (18). The original resonant frequencies ω_{RX} are determined once the receiving loop is designed. To charge to different numbers of loads in a stable manner, the combined frequency $(\omega_{\mathrm{RX}}/\sqrt{1+\sum_{j'=1}^{n} k_{\mathrm{ij}'}})$ of multiple receiving coils is supposed to be constant. When the parameters of each receiver are fixed, the only feasible way to achieve this goal is to adjust the distributions of the receiving coils. Nevertheless, the relationship between the combined frequency and the distributions is nonlinear, requiring more analysis.

The system structure of helical coils placed on a surface is shown in Fig. 5.

According to Neumann's Formula, the coupling coefficient is defined as follows:

$$k_{12} = \frac{\mu_0 N_1 N_2}{4\pi\sqrt{L_1 L_2}} \int_0^{2\pi} \mathrm{d}\phi \int_0^{2\pi} \frac{r_1 r_2 \cos(\theta-\phi)\mathrm{d}\theta}{\sqrt{(r_2\cos\theta - r_1\cos\phi)^2 + (r_2\sin\theta - r_1\sin\phi + r_{12})^2}}. \tag{19}$$

It can be seen from (19) that the only factor affecting the coupling coefficient is the distance between coil centers r_{12} when the coil parameters are determined. To carry out more subtle analysis, we substitute k_{ij} in (19) by $f(r_{\mathrm{ij}})$.

The uniform output power can be achieved according to the specific distribution schemes of different numbers of receiving coils ($3 \le n \le 6$), as presented in Fig. 3. The sum of coupling coefficients between one receiving coil and other receiving coils is tabulated in Table I. The radius of circumscribed circles, in which all the receiving coils are distributed, is represented by r. The radius of each receiving coil is denoted by a. Restrictions should be met to avoid overlap between the receiving coils.

It aims to determine the relationship between r and the number of receiving coils, which can achieve constant $\sum_{j'=1}^{n} k_{\mathrm{ij}'}$. The quantitative analysis of $\sum_{j'=1}^{n} k_{\mathrm{ij}'}$ in accordance with r for different numbers of receiving coils is presented in Fig. 4. Specific system parameters are shown in Table II.

Fig. 6 contains four situations in which n changes from 3 to 6, where the curves denote the theoretical calculations and the dots show actual measurements. According to the constraint conditions of Table I, when there are three receiving coils, the

TABLE I
Sum of Coupling Coefficients ($\sum_{j'=1}^{n} k_{\mathrm{ij}'}$)

Number of receiving coils (n)	Composite figure	$\sum_{j'=1}^{n} k_{\mathrm{ij}'}$	Constraint conditions
3	Equilateral triangle	$2f(\sqrt{3}r)$	$r \ge 2a/\sqrt{3}$
4	Square	$2f(\sqrt{2}r) + f(2r)$	$r \ge \sqrt{2}a$
5	Regular pentagon	$2f(2r\sin\frac{\pi}{5}) + 2f(2r\sin\frac{2\pi}{5})$	$r \ge a/\sin\frac{\pi}{5}$
6	Regular hexagon	$2f(r) + 2f(\sqrt{3}r) + f(2r)$	$r \ge 2a$

TABLE II
Actual Parameters of Receiving Coils

Parameter	Value
Turns	10
Radius a (cm)	5
Wire	Liz wire-1650/0.05F
The way of winding	Tight winding
Self-inductance(μH)	24.34

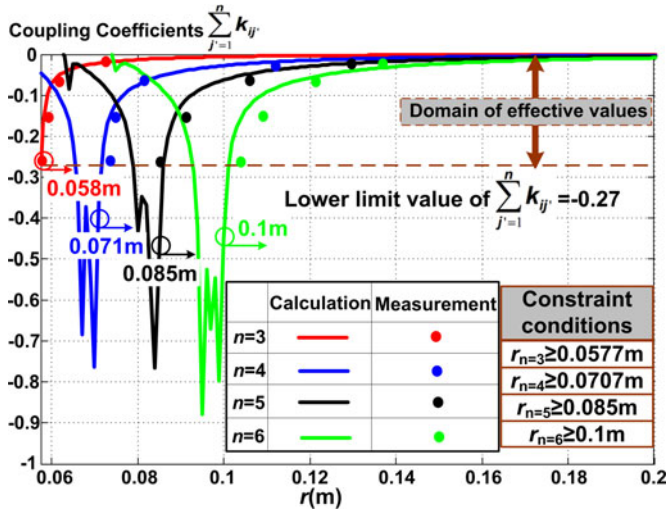

Fig. 6. Sum of coupling coefficients ($\sum_{j'=1}^{n} k_{\mathrm{ij}'}$) changes with the radius (r) of the circumscribed circles, in which all receiving coils are distributed.

$$\mathbf{I} = \frac{U_s k_{\mathrm{tr}} k \cdot \sqrt{L_t / L_i}}{(nk^2 - 1/Q_r Q_i)\left[R_{\mathrm{st}} + j\omega_r L_t (1 - {\omega_{\mathrm{TX}}}^2/{\omega_r}^2)\right] - k_{\mathrm{tr}}\sqrt{L_t/L_r} R_{iL} L_t / L_i} \tag{15}$$

TABLE III
ACTUAL PARAMETERS OF RCS AND SYSTEM

Parameter	Value	Parameter	Value
Turns	20	k_{tr}	0.11
Radius a(cm)	25	d_{ri}	0.3
Wire	Liz wire-1650/0.05F	U_s (V)	20
Self-inductance(μH)	176.4	R_L (Ω)	7.3
d_{tr} (m)	0.4	P_{min} (W)	5

radius(r) of the circumscribed circles should be larger than $2a/\sqrt{3}$, where a is the radius of each receiving coil. Table II gives the specific parameters of each receiving coil, that is, $a = 5$ cm. So, the radius(r) of the circumscribed circles must be greater than 0.058 m. In Fig. 6, the adjustment range of the coupling coefficient is set, that is, the domain of effective values, in which the 0.058 m is the lower limit value. Using any red dot as a reference, other three dots are on a contour line with the reference. The outflow direction of magnetic field marked "+" in Fig. 5 is set as the positive direction of mutual inductance calculation. The coupling coefficients are negative because the positive direction of mutual inductance calculation has been prespecified. In this paper, the mutual inductance between two coils is measured by the method of the bridge balance. The corresponding coupling coefficient can be further calculated based on the mutual inductance. It has been verified in [30] that high accuracy and precision can be guaranteed. In the measurement, taking the dotted terminals of the receiving coils into account, the measured values of the mutual inductances are all negative. The measured results are consistent with the analytical calculations as shown in (19), which demonstrating the correctness of the theoretical analysis. It is observed that several combinations of number of coils and circumscribed circles radii are qualified to make the operating frequency constant when $\sum_{j'=1}^{n} k_{\mathrm{ij}'}$ ranges from –0.27 to 0; besides, we can get a series of new functions expressed by $r_{\mathrm{I}} = f(n)$ with function fitting, which involve the radius(r) of the circumscribed circles and the number(n) of loads.

B. Optimization of Output Power Stabilization

According to (17), a constant $|\mathbf{I}|$ is necessary to stabilize the receiving power when the number of receiving coils changes to meet the minimal load demand P_{min}; therefore, the following constraints are needed:

$$\begin{cases} \left(nk - \dfrac{1}{kQ_rQ_i}\right) R_{\mathrm{st}} - \dfrac{k_{\mathrm{tr}}\sqrt{L_t/L_r}R_L L_t/L_i}{k} = \xi \\ |\xi| \leqslant U_s k_{\mathrm{tr}} \sqrt{\frac{L_t R_L}{L_i P_{\mathrm{min}}}} \end{cases} \quad (\xi \in \mathbb{R}) \tag{20}$$

where the constant ξ is used to maintain charging power stability. If the axial distance between the RC and the receiving coils is fixed, the coupling coefficient between the RC and each receiving coil can be calculated as a function of distribution radius (r). Here, the TC and the RC with the same parameters are used and the component values are displayed in Table III.

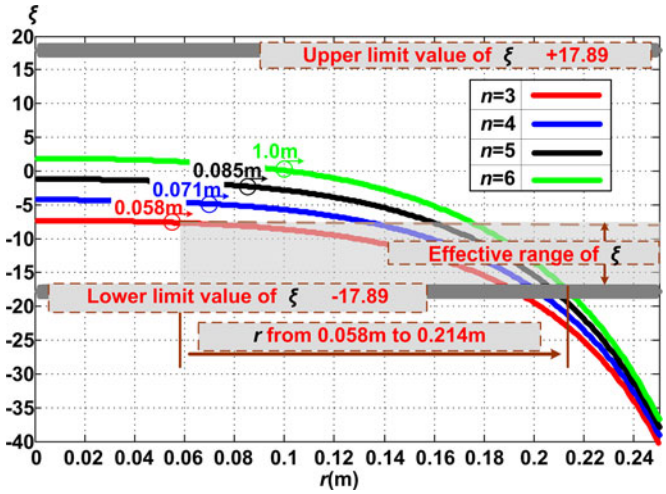

Fig. 7. Constant ξ changes with the radius (r) of the circumscribed circles.

According to Table III, the constant ξ ($3 \leq n \leq 6$ for instance), which could satisfy the power demand of each load and keep the charging power unchanged, has been provided, as shown in Fig. 7.

In Fig. 7, when the ξ stays between the upper limit value and the lower limit value, the received power can meet the demand of the load. In the designed system, the upper and lower limits of ξ are $\pm$17.89. When the number of loads changes, there are several constants, which would make the load charging power constant; in the meanwhile, the range of acceptable radii r is expressed as [0.058 m, 0.214 m]. With regard to Figs. 3 and 7, it can be concluded that the charging power for each load can be stabilized by transforming the distributions of receivers. To stabilize the charging power when the number of receiving coils changes, the radius of the circumscribed circles shall be adjusted accordingly. With the proposed strategy, large charging power fluctuations can be avoided and thus contributes to longer battery life-expectancy. The combinations of number of coils and distribution radius, namely the real number pair (n, r), are preferred to keep the charging power stable, as shown in Fig. 7. Similar to the description in the optimization of efficiency, a series of new functions expressed by $r_{\mathrm{II}} = f(n)$ may be obtained by function fitting, which concern the radius(r) of the circumscribed circles and the number (n) of loads.

The ideal performance of the proposed WPT system can be achieved by meeting $r_{\mathrm{I}} = f(n)$ and $r_{\mathrm{II}} = f(n)$. Nevertheless, it is hard to implement the design to meet both constraints; therefore, the absolute difference value between r_{I} and r_{II} is designed to be as small as possible, which can be illustrated by

$$|r_{\mathrm{I}} - r_{\mathrm{II}}| \leqslant \kappa \quad (\kappa \in \mathbb{R}). \tag{21}$$

Here, κ, defined as an acceptable value, could make the operating frequency and the output power quasi-constant. In (21), κ is set to 1 cm. A series of curves of r_{I} and r_{II} in the proposed WPT system is displayed in Fig. 8.

As illustrated previously in Fig. 8, the solid lines (r_{I}) represent the curve cluster that makes the operating frequency constant

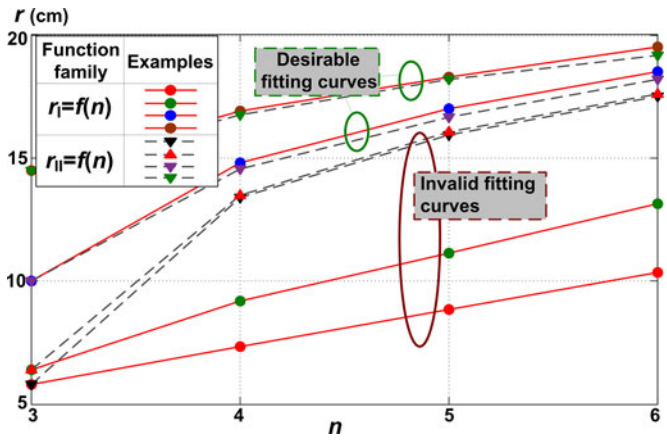

Fig. 8. Fitting curves for the radius (r) of the circumscribed circles and the number (n) of loads.

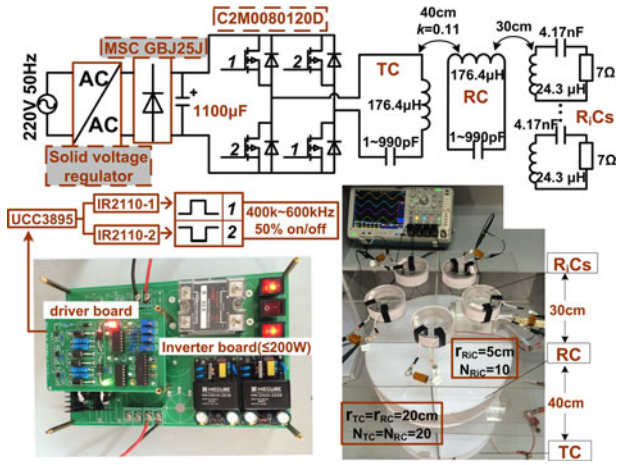

Fig. 9. Experimental device.

and the dotted lines ($r_{\rm II}$) express the curve cluster that could make the charging power for each load constant, even though the number of the loads changes. The two cluster curves, covered by green circles, are described as desirable fitting curves, where all the corresponding (n, r) pairs can guarantee that both the operating frequency and the load power are constant. However, it should be understood that different kinds of loads may present different antifluctuation abilities to the charging power; therefore, the κ can be selected thus: a bigger κ refers to more combinations of (n, r). Although the desirable fitting curves shown in Fig. 8 are just typical examples, the optimization strategy used in this paper could be applied to other multiload systems as well.

V. Experimental Results

Two experimental prototypes, designed for the WPT system with a single RC, are implemented to verify the aforementioned analysis, in which, the first part of the experiment is carried out with a single load and the other is focused on better illustrating frequency responses and arrangement of multiple loads. The topologies of the transfer system are similar to those shown in Figs. 1 and 4. Tables II and III list the specific system parameters. A power source with a full-bridge invertor structure is adopted in the experiment. The CREE SiC MOSFET C2M0080120D is used as active switch of the voltage-source inverter (VSI), and the TI UCC3895 is used as the phase-shift pulse width-modulated controller for the VSI. Two IR2110 are used as chips in the driver. The transmitter, the relay, and the receiver inductors are spiral coils, composed of tightly wound Litz wires of the diameter of 3.3 mm. Both the TC and the RC are connected in series with low-loss CKTB adjustable ceramic vacuum capacitors as compensating capacitors. The regulation precision of the compensating capacitors can reach 0.1 pF and makes it possible to regulate the resonant frequencies of the TC loop and the RC loop. The receiving coil is connected with a fixed CBB capacitor in series, providing a fixed resonant frequency. The inductances, the capacitances, the resistances, and the self-resonant frequencies are measured by R&S ZNB8 vector network analyzers. Tektronix MDO4054B-3 oscilloscope linked to an Agilent DSO5014A oscilloscope to measure the voltage and the current of each load when there are more than five loads. The type of high-frequency current probe is an Agilent N2782A, which measured with a conversion ratio of 0.1 V/A. The transfer efficiency from the transmitter to the receiver, and the load power, are not measured directly. Instead, these performance indices are calculated from the measured voltages and currents. The photograph of the experimental prototype is shown in Fig. 9.

A. Experiment With Single Load

1) Experimental Plan and Steps: This part is intended to verify the relationship between the operating frequency and the self-resonant frequency of each coil loop to achieve the maximum efficiency and the output power even when the coupling is very weak. The experiment follows these steps: 1) the self-resonant frequencies of the TC loop and the receiving coil loop are set to 480 and 500 kHz, respectively. The self-resonant frequency of RC loop is set to 520 and 500 kHz. The output power and the transfer efficiency are then measured at different operating frequencies. 2) The self-resonant frequencies of both the RC loop and the receiving coil loop are set to 500 kHz. The resonant frequency of the TC loop is set to 480, 500, and 520 kHz, respectively. The output power and the transfer efficiency are then measured using the method outlined in Step 1.

2) Experimental Results: The output voltage of source power is 20 V and operating frequency can be regulated from 410 to 600 kHz. The mutual inductance is measured by R&S ZNB8 vector network analyzers. The coupling coefficient between the TC and the RC is $k_{\rm tr} = 0.11$ and the coupling coefficient between the RC and the receiver is $k_{r1} = 0.07$. The receiving power of the load is calculated based on the measured RMS value of load voltage. Some experimental results are shown in Fig. 10(a)–(c). The waveforms in each figure are expressed by the load voltage (V_L) and the input current, which can be understood as the current in the TC (I_t). The input current is measured by an Agilent N2782A, which used a conversion ratio of 0.1 V/A.

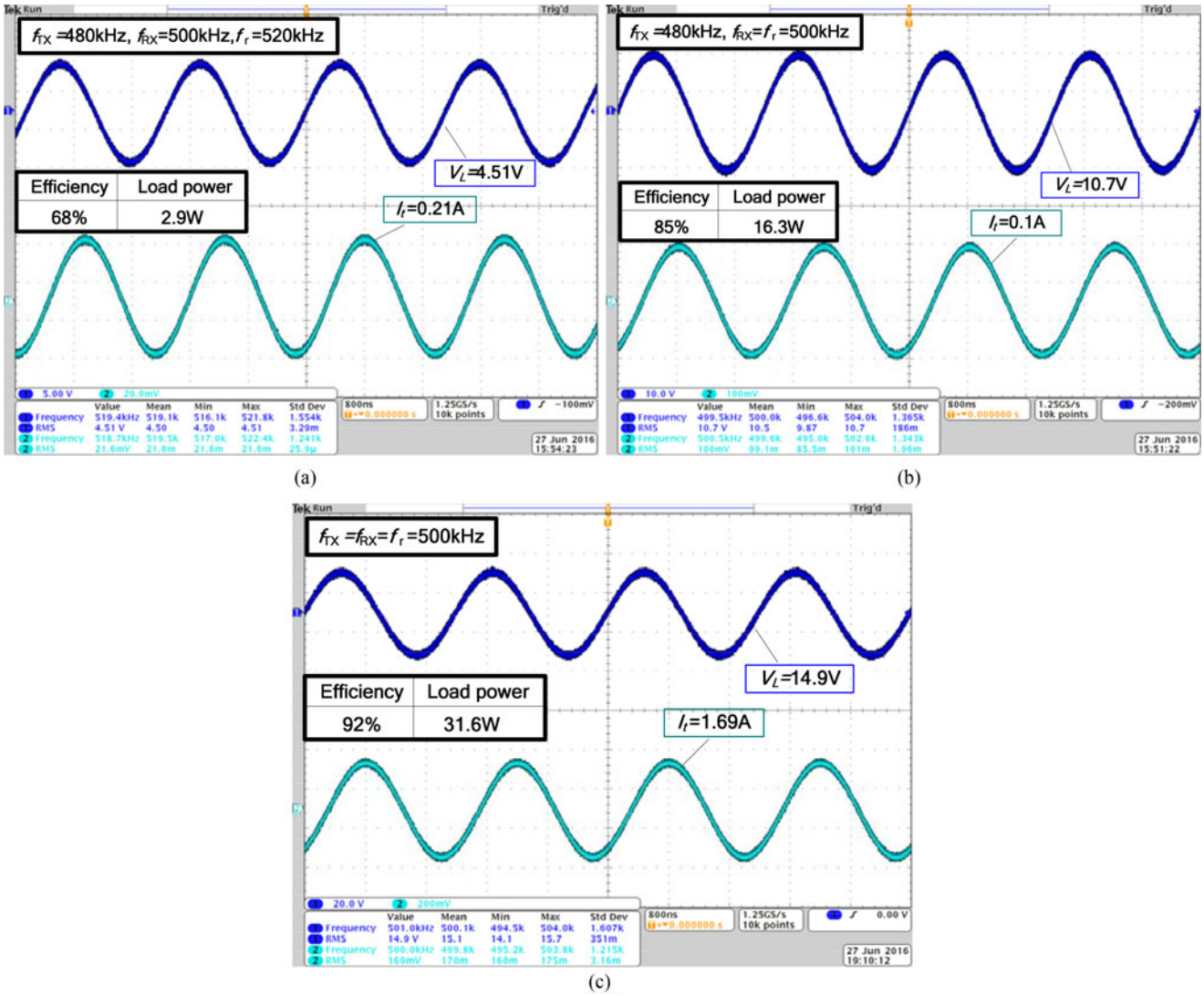

Fig. 10. Typical experimental results with a single load. (a) Original resonant frequencies of the TC, RC, and R_1C are different. (b) Original resonant frequencies of the RC and R_1C are equal. (c) All the original resonant frequencies of coils are the same.

In Fig. 10(a)–(c), the load receiving power and the transfer efficiency are measured in three frequency cases. To verify the correctness of the theory in more detail, all experimental results from Steps 1 and 2 are shown in Fig. 11(a) and (b), respectively.

As shown in Fig. 11, it is shown that the proposed operating frequency could produce peak performances when the couplings between the RC and the TC, or between the RC and the R_1C, are fixed. Fig. 11(a) shows that the maximum transfer efficiency and output power are achieved at $f = f_r = 520$ kHz when the self-resonant frequencies of the TC, RC, and R_1C differ from each other. It is demonstrated that both the transfer efficiency and the output power are determined by the original resonant frequency of the RC, which is represented as f_r. There are two extreme points of frequency at $f = f_r$ and $f = f_{\rm TX}$ where the maximum output power can be achieved. It validates the finding that the effect of self-resonant frequencies of the TC and the RC on output power still dominates even though the coils share different self-resonant frequencies. In case of $f = f_r = f_{\rm RX} = 500$ kHz, the transfer efficiency is maximized according to (4). The measured results show that the maximum transfer efficiency is 85% and the output power reaches 16.3 W. The system performance is enhanced drastically while compared with the nonresonant case where the transfer efficiency is 68% and the output power is 2.9 W. Experimental results in Fig. 11(b) show that the maximum transfer efficiency is maximized when $f = f_r = f_{\rm RX} = 500$ kHz, regardless of the self-resonant frequency of the TC, which is consistent with (4). The output power is maximized only when $f = f_r = f_{\rm RX} = f_{\rm TX} = 500$ kHz as illustrated by (7); specifically, 31.6 W is achieved in this experiment.

B. Experiment With Multiple Loads

1) Experimental Plan and Steps: This part is designed to demonstrate the feasibility of achieving the maximum transfer efficiency and the constant output power in the proposed WPT system with multiple receivers: the original resonant frequencies

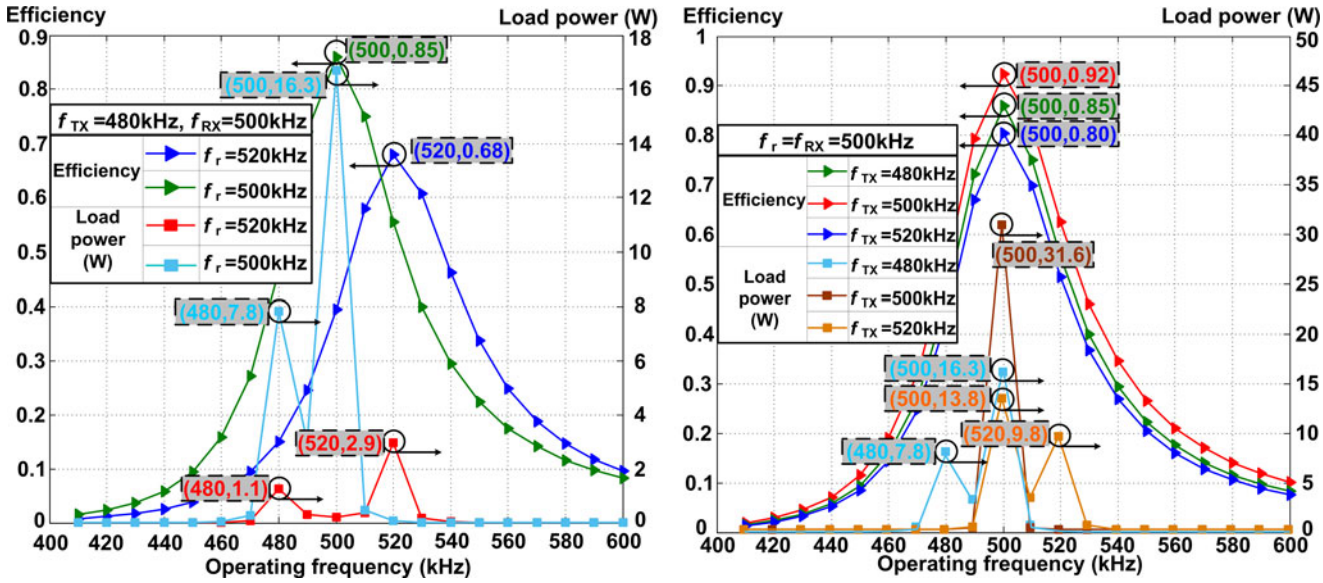

Fig. 11. Efficiency and transfer power versus operating frequency. (a) Original resonant frequencies of the TC and the R_1C are 480 and 500 kHz, respectively. The original resonant frequency of the RC is set to 520 or 500 kHz. (b) Original resonant frequencies of the RC and R_1C are both 500 kHz; the original resonant frequency of the TC is chosen as 480, 500, or 520 kHz, respectively.

of the receivers are all the same. Specific experimental setups are shown as follows: 1) four receivers are used and the distribution radius is determined at random according to Fig. 6 (such as $r = 7.5$ cm and $\sum_{j'=1}^{n} k_{ij'} = 0.14$). The original resonant frequencies of the TC and the receiver are 480 and 500 kHz, respectively. The original resonant frequencies of the RC are set to 468 and 500 kHz, respectively, to investigate the effect of operating frequency on transfer efficiency and output power. 2) The original resonant frequencies of the RC and the receiver are 468 and 500 kHz. The original resonant frequencies of the TC are set to 468 and 500 kHz, respectively, to investigate the effect of the operating frequency on transfer efficiency and output power. 3) The original resonant frequency of the receiver is set to 500 kHz and that of other coils needs to be regulated by (18). The charging power of each load and the optimized operating frequency, varied with the circumscribed circle radii, are measured.

2) Experimental Results: The output voltage of the source power is 20 V and the operating frequency can be regulated from 410 to 580 kHz. Typical measurements are shown in Fig. 12(a)–(d). The waveforms in each figure represent the voltage at each load. The input current is directly measured and marked in each figure.

In order to verify the correctness of the theory in more detail, all experimental results of Steps 1 and 2 are shown in Fig. 13(a) and (b), respectively.

In Fig. 13, it is shown that there is a proposed operating frequency, which could make the WPT system with four receiving coils produce peak performances when the original resonant frequencies of the R_iC and TC, or that of the RC and R_iC, are fixed at the same time. Fig. 13(a) shows that the maximum transfer efficiency is only 77% when the self-resonant frequencies of the RC and the receivers do not satisfy (13), which is much smaller than the maximum transfer efficiency of 87% when the frequencies of coils conform to (13). The measured frequencies are $f \cong f_r \cong f_{\mathrm{RX}}/\sqrt{1+\sum_{j'=1}^{n} k_{ij'}} \cong 470\,\mathrm{kHz}$, indicating a deviation of 2 kHz resulting from measurement errors and low-quality factors.

In Fig. 13(b), the maximum transfer efficiency is reached at $f = 470$ kHz when the original resonant frequencies of the RC loop and the receivers satisfy (13), proving the correctness of the theoretical analysis. In addition, the maximum output power reaches 63.2 W when the self-resonant frequency of the TC satisfies the maximum power condition, as shown in (18). The receiving power of each receiver is 15.8 W, which can meet the demands of practical applications.

In summary, the system's overall efficiency (η_{oal}) is the product of the inverter efficiency and the transfer efficiency of power delivered from the TC to the load, which are expressed as η_{ivt} and η_{t-l}, respectively. The aforementioned efficiency is the transfer efficiency (η_{t-l}). The overall efficiency (η_{oal}) can be calculated according to (22). As a result, the overall efficiency reaches 84.6% by taking the inverter efficiency of about 91% into account

$$\eta_{\mathrm{oal}} = \eta_{\mathrm{ivt}} \cdot \eta_{t-l}. \tag{22}$$

Based on the said analysis, the optimal operating frequency and the charging power will also vary with the number of loads. At this point, we need to configure the distribution radius of the loads to make the optimal operating frequency and the charging power both constant. Taking the three loads system and the four loads system as the examples, the distribution radius of the three loads system is set to 16 cm, where $\sum_{j'=1}^{n} k_{ij'} = 0.004$ and the theoretical value of the optimal operating frequency is 499 kHz. In order to ensure that the optimal operating frequency remains stable while adding a load, the distribution radius of four receiving coils is required in the range of 17–19 cm. When the

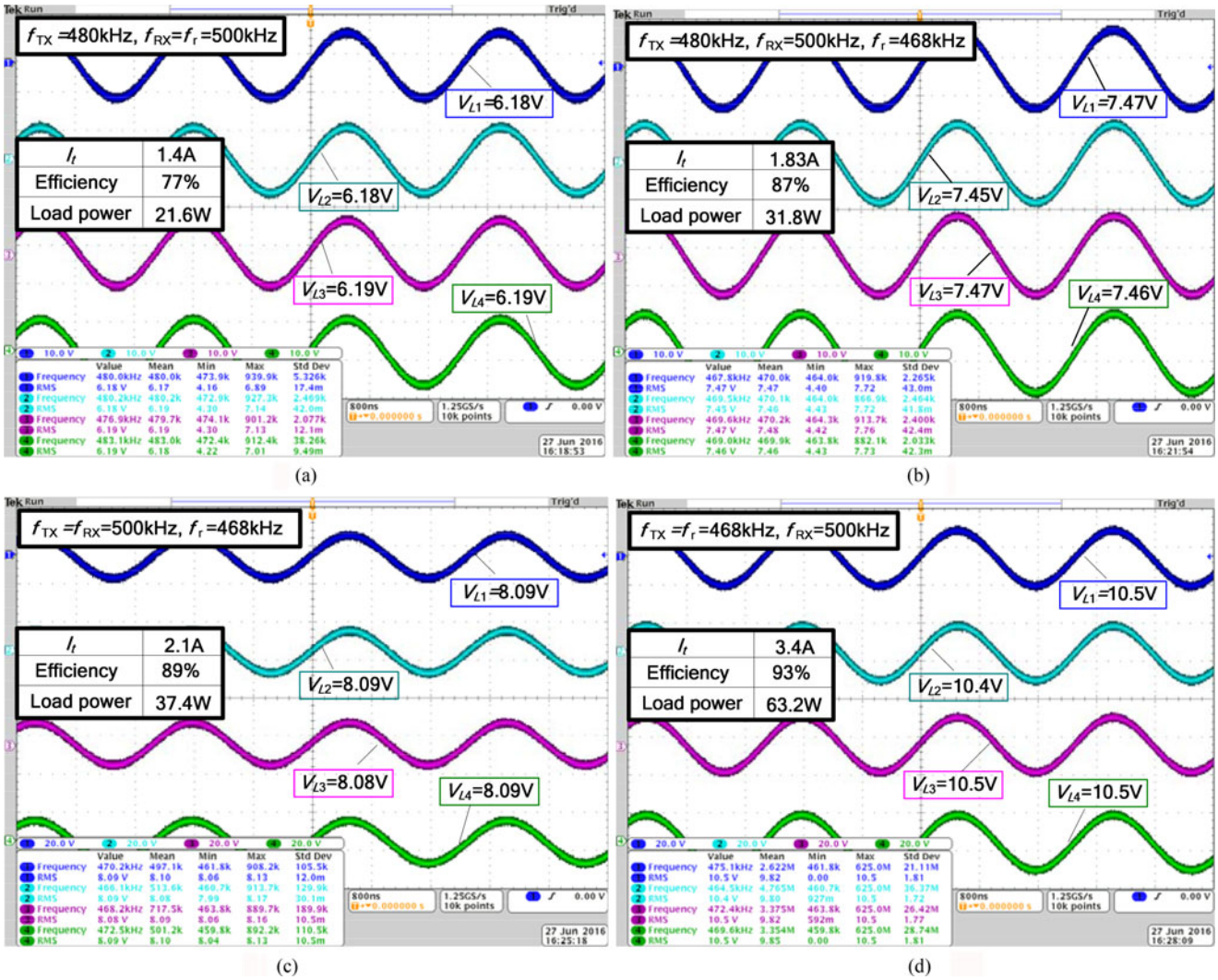

Fig. 12. When $r = 7.5$ cm, partial results showing the load voltages versus the operating frequency in a four load system. (a) Original resonant frequencies of the TC, RC, and R_iC do not satisfy (13). (b) Original resonant frequencies of the RC and R_iC satisfy (13) but do not meet (18). (c) Same condition as (b) except with regard to the original resonant frequencies of the TC. (d) Original resonant frequencies of the coils meet (18).

distribution radius of the receiving coils changes to 18 cm, the charging power for each load in the four receiving coils system is basically consistent with that of the three receiving coils system. The experimental results are shown in Fig. 14(a) and (b).

In the two cases, when the number of the receiving coils changes from 3 to 4, by adjusting the radius(r) of the circumscribed circles from 16 to 18 cm, the difference between the optimal operating frequencies of the two systems is only 2 kHz and the maximum fluctuation of the charging power for a single load is only 0.1 W. The theoretical analysis has been verified well. However, when the number of the receiving coils is more than 4, the voltage waveform of each load cannot be fully displayed in the oscilloscope. In order to avoid confusion, the operating frequencies and the receiving powers, which have been measured when the number of the loads varies from 3 to 6, are summarized in Fig. 15. The situation in Step 3 is also discussed in Fig. 15 to verify that the operating frequency and the receiving power of each load can be stabilized by adjusting the radius(r) of the circumscribed circles when the number of the loads changes.

In Fig. 15, the original resonant frequency of each receiving coil is constant at 500 kHz. The area, covered by the blue dashed box, spans $r \in [12, 20]$. It can not only maintain the optimal operating frequency unchanged, but guarantee that the charging power is constant. Different optimal operating frequencies correspond to different array radii ($r_{n=3}$, $r_{n=4}$, $r_{n=5}$, $r_{n=6}$) and load powers. It can be concluded that the smaller the distribution radius, the larger the change rates of optimal operating frequency and output power caused. Under this condition, it is infeasible to stabilize the operating frequency and the receiving power by means of adjusting distribution radii; however, the change rates decrease as for larger distribution radii. If the receiving power fluctuation of 1 W is allowed, as represented by $\Delta P \leq 1$ W in Fig. 15, several combinations of the number of coils and the distribution radius (n, r) can realize the goal of stabilizing the output power and the optimized operating

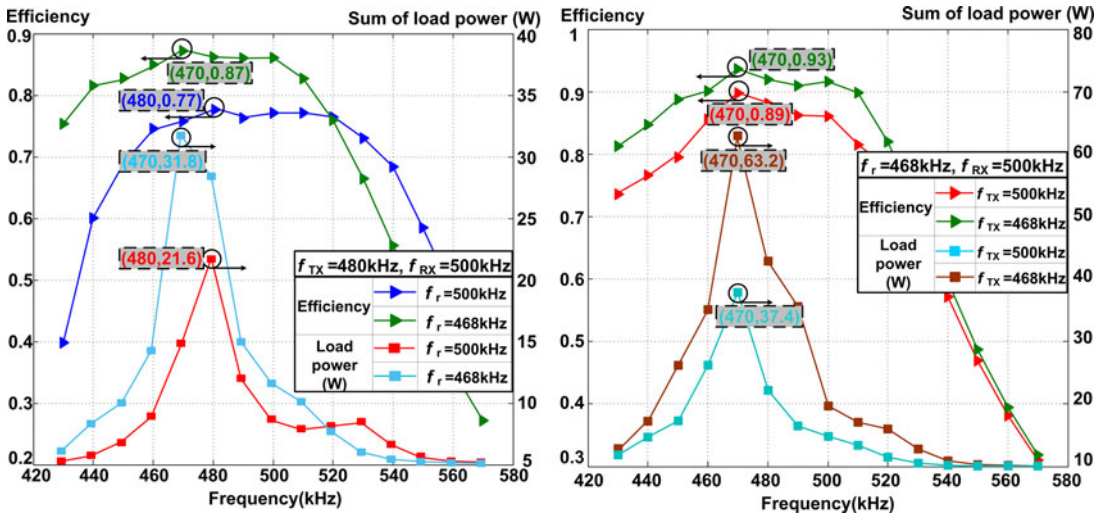

Fig. 13. Efficiency and sum of load powers versus operating frequency. (a) Original resonant frequencies of the TC and R_iC are 480 and 500 kHz, respectively. The original resonant frequency of the RC is set to 468 or 500 kHz. (b) Original resonant frequency of the RC is 468 kHz and that of the R_iC is 500 kHz. The original resonant frequency of the TC is chosen as either 468 or 500 kHz.

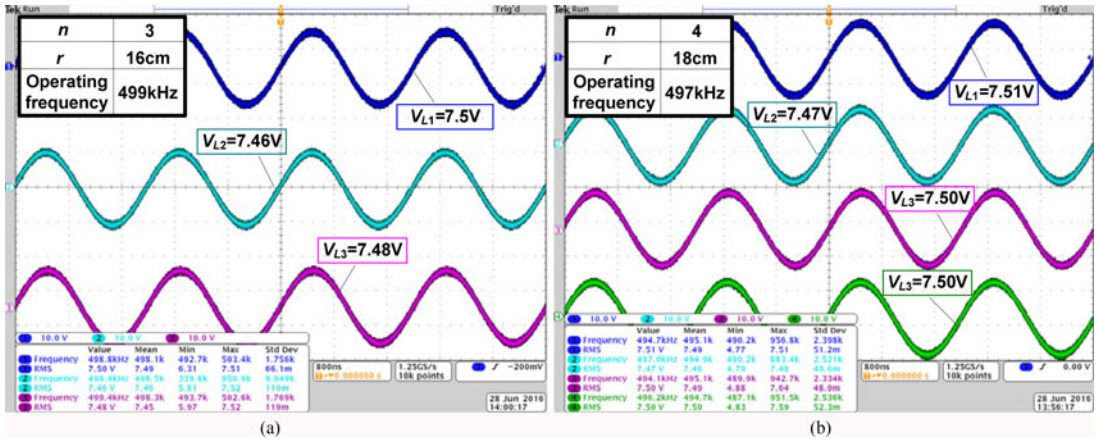

Fig. 14. Effect of the optimal distribution radius on operating frequency and charging power. (a) $n = 3$, $r = 16$ cm. (b) $n = 4$, $r = 18$ cm.

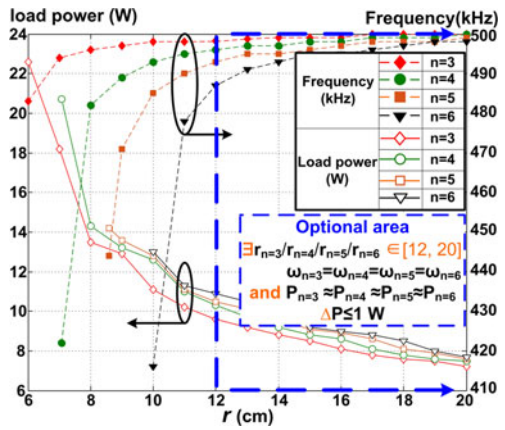

Fig. 15. Operating frequency and charging power for each load versus the radius (r) of the circumscribed circles.

frequency. For instance, the optimal distribution radius becomes 12, 15, 17, and 18 cm as the number of receivers changes from 3 to 6. At this point, the measured results show that the load powers are all 9 ± 0.3 W. If the operating frequencies and receiving powers of $n = 3$ and $n = 4$ in Fig. 14 are set as references, the radii of the circumscribed circles, the operating frequencies, and the receiving powers of $n = 5$ and $n = 6$ can be determined in Fig. 15, which are expressed as (19 cm, 497 kHz, 8.01 W) and (19 cm, 496 kHz, 8.05 W), respectively. In comparison, we know that the operating frequency is constrained in the range of 496–499 kHz. Besides, the maximum error of receiving power is 0.1 W. The experimental results above validate that the goal of making both the system operating frequency and the output power stable can be achieved just by choosing the right real number pair of (n, r).

Although the measurements are performed only for specific sets of dimensions, distance, center frequency, inductance/capacitance, and source/load impedances, the conclusions in Sections II–IV can still apply to other situations in general.

VI. Conclusion

As for the three-coil WPT system with single load or multiple loads, a method of configuring the operating frequency and

the self-resonant frequencies of coils to optimize the transfer efficiency and the output power is proposed. When charging for multiple loads, the impact of coupling coefficients between receivers on the maximum transfer efficiency and the maximum output power is analyzed; besides, the distribution method of the receivers according to the number of loads is also proposed, which could provide identical and stable power for loads and keep the optimized frequency stable. A comprehensive analysis has been included to explain this optimal WPT power control method. The effectiveness of the proposed methods of power stabilization based on the efficiency optimization for WPT systems with a single relay by frequency configuration and distribution design of receivers have been successfully evaluated with simulation studies and practically confirmed with a hardware setup. It should be noted that the optimal methods could not only apply to the WPT systems proposed in this paper but to the systems with different structures (multiple RCs, multiple receiving coils) and parameters, which provide a simple, but effective solution to restrain output power fluctuation and simplify source control.

REFERENCES

[1] H. J. Choi, E. H. Ahn, S. Y. Park, and J. R. Choi, "Portable battery charging circuits for enhanced magnetic resonance wireless power transfer (WPT) system," in *Proc. 9th Conf. Ph.D. Res. Microelectron. Electron.*, 2013, pp. 273–276.

[2] J. Kim, D.-H. Kim, J. Choi, K.-H. Kim, and Y.-J. Park, "Free-positioning wireless charging system for small electronic devices using a bowl-shaped transmitting coil," *IEEE Trans. Microw. Theory Techn.*, vol. 63, no. 3, pp. 791–800, Mar. 2015.

[3] J. Hirai, T.-W. Kim, and A. Kawamura, "Study on intelligent battery charging using inductive transmission of power and information," *IEEE Trans. Power Electron.*, vol. 15, no. 2, pp. 335–345, Mar. 2000.

[4] X. Li, X. Meng, C. Y. Tsui, and W. H. Ki, "Reconfigurable resonant regulating rectifier with primary equalization for extended coupling and loading-range in bio-implant wireless power transfer," *IEEE Trans. Biomed. Circuits Syst.*, vol. 9, no. 6, pp. 875–884, Dec. 2015.

[5] J. D. Kim, C. Sun, and I. S. Suh, "A proposal on wireless power transfer for medical implantable applications based on reviews," in *Proc. IEEE Wireless Power Transf. Conf.*, 2014, pp. 166–169.

[6] S. Bilicz, S. Gyimóthy, J. Pávó, L. L. Tóth, Z. Badics, and B. Bálint, "Modeling of resonant wireless power transfer with integral formulations in heterogeneous media," *IEEE Trans. Magn.*, vol. 52, no. 3, pp. 1–4, Mar. 2016.

[7] K. Hatanaka *et al.*, "Power transmission of a desk with a cord-free power supply," *IEEE Trans. Magn.*, vol. 38, no. 5, pp. 3329–3331, Sep. 2002.

[8] C. Yang and K. Tsunekawa, "Study of WPT system for charging portable devices on a desk," in *Proc. 10th Int. Symp. Antennas Propag. EM Theory Conf.*, 2012, pp. 320–324.

[9] *Qi System Description: Wireless Power Transfer, Volume I: Low Power, Part 1: Interface Definition, Wireless Power Consortium, version 1.1*, Apr. 2012.

[10] M. Mcdonough, "Integration of inductively coupled power transfer and hybrid energy storage system: A multiport power electronics interface for battery-powered electric vehicles," *IEEE Trans. Power Electron.*, vol. 30, no. 11, pp. 6423–6433, Nov. 2015.

[11] S. Kim, H. H. Park, J. Kim, J. Kim, and S. Ahn, "Design and analysis of a resonant reactive shield for a wireless power electric vehicle," *IEEE Trans. Microw. Theory Techn.*, vol. 62, no. 4, pp. 1057–1066, Apr. 2014.

[12] S. Y. Choi, B. W. Gu, S. Y. Jeong, and C. T. Rim, "Advances in wireless power transfer systems for roadway-powered electric vehicles," *IEEE J. Emerg. Sel. Topics Power Electron.*, vol. 3, no. 1, pp. 18–36, Mar. 2015.

[13] J. H. Kim *et al.*, "Development of 1-MW inductive power transfer system for a high-speed train," *IEEE Trans. Ind. Electron.*, vol. 62, no. 10, pp. 6242–6250, Oct. 2015.

[14] T. Imura and Y. Hori, "Maximizing air gap and efficiency of magnetic resonant coupling for wireless power transfer using equivalent circuit and Neumann formula," *IEEE Trans. Ind. Electron.*, vol. 58, no. 10, pp. 4746–4752, Oct. 2011.

[15] A. P. Sample, D. T. Meyer, and J. R. Smith, "Analysis, experimental results, and range adaptation of magnetically coupled resonators for wireless power transfer," *IEEE Trans. Ind. Electron.*, vol. 58, no. 2, pp. 544–554, Feb. 2011.

[16] A. Kurs, A. Karalis, R. Moffatt, J. D. Joannopoulos, P. Fisher, and M. Soljacic, "Wireless power transfer via strongly coupled magnetic resonances," *Science*, vol. 317, pp. 83–86, Jul. 2007.

[17] W. X. Zhong, K. L. Chi, and S. Y. Hui, "Wireless power domino-resonator systems with noncoaxial axes and circular structures," *IEEE Trans. Power Electron.*, vol. 27, no. 11, pp. 4750–4762, Nov. 2012.

[18] S. C. Moon, B. C. Kim, S. Y. Cho, C. H. Ahn, and G. W. Moon, "Analysis and design of a wireless power transfer system with an intermediate coil for high efficiency," *IEEE Trans. Ind. Electron.*, vol. 61, no. 11, pp. 5861–5870, Nov. 2014.

[19] W. X. Zhong, C. Zhang, X. Liu, and S. Y. R. Hui, "A methodology for making a three-coil wireless power transfer system more energy efficient than a two-coil counterpart for extended transfer distance," *IEEE Trans. Power Electron.*, vol. 30, no. 2, pp. 933–942, Feb. 2015.

[20] J. Zhang, X. Yuan, C. Wang, and Y. He, "Comparative analysis of two-coil and three-coil structures for wireless power transfer," *IEEE Trans. Power Electron.*, vol. 32, no. 1, pp. 341–352, Jan. 2017.

[21] V. T. Nguyen, S. H. Kang, J. H. Choi, and C. W. Jung, "Magnetic resonance wireless power transfer using three-coil system with single planar receiver for laptop applications," *IEEE Trans. Consum. Electron.*, vol. 61, no. 2, pp. 160–166, May 2015.

[22] M. Fu, H. Yin, X. Zhu, and C. Ma, "Analysis and tracking of optimal load in wireless power transfer systems," *IEEE Trans. Power Electron.*, vol. 30, no. 7, pp. 3952–3963, Jul. 2015.

[23] Q. Yuan, Q. Chen, J. Li, and K. Sawaya, "Optimum load of WPT system analyzed by S-parameters," in *Proc. Eur. Conf. Antennas Propag.*, 2012, pp. 3604–3608.

[24] E. Bou, R. Sedwick, and E. Alarcon, "Maximizing efficiency through impedance matching from a circuit-centric model of non-radiative resonant wireless power transfer," in *Proc. IEEE Int. Symp. Circuits Syst. Conf.*, 2013, pp. 29–32.

[25] D. Ahn and S. Hong, "Effect of coupling between multiple transmitters or multiple receivers on wireless power transfer," *IEEE Trans. Ind. Electron.*, vol. 60, no. 7, pp. 2602–2613, Jul. 2013.

[26] L. Sun, H. Tang, and S. Zhong, "Load-independent output voltage analysis of multiple-receiver wireless power transfer system," *IEEE Antennas Wireless Propag. Lett.*, vol. 15, pp. 1238–2241, Apr. 2016.

[27] K. E. Koh, T. C. Beh, T. Imura, and Y. Hori, "Impedance matching and power division using impedance inverter for wireless power transfer via magnetic resonant coupling," *IEEE Trans. Ind. Appl.*, vol. 50, no. 3, pp. 2061–2070, May/Jun. 2014.

[28] K. Lee and D. H. Cho, "Analysis of wireless power transfer for adjustable power distribution among multiple receivers," *IEEE Antennas Wireless Propag. Lett.*, vol. 14, pp. 950–953, 2015.

[29] M. Schuetz, A. Georgiadis, A. Collado, and G. Fischer, "A particle swarm optimizer for tuning a software-defined, highly configurable wireless power transfer platform," in *Proc. IEEE Wireless Power Transf. Conf.*, 2015, pp. 1–4.

[30] J. F. Zhao, X. L. Huang, and W. Wang, "Wireless power transfer with two-dimensional resonators," *IEEE Trans. Magn.*, vol. 50, no. 1, pp. 1–4, Jan. 2014.

Wei Wang was born in Nanjing, China, in 1988. He received the B.S. degree in electrical engineering and automation from Jiangnan University, Wuxi, China, in 2007, and the M.S. degree in electrical engineering from Southeast University, Nanjing, in 2013, where he is currently working toward the Ph.D. degree in electrical engineering.

Since 2011, his research interests mainly focus on numerical methods of electromagnetic field computation and novel wireless power transfer systems.

Xueliang Huang (M'11) was born in Zhoushan, China, in 1969. He received the B.S., M.S., and Ph.D. degrees in electrical engineering from Southeast University, Nanjing, China, in 1991, 1994, and 1997, respectively.

From 2002 to 2004, he was with the University of Tokyo as a Postdoctoral Researcher. Since 2004, he has been a Professor in the Department of Electrical Engineering, Southeast University. He is the author of four books, more than 150 articles, and more than 40 inventions. His research interests include novel wireless power transfer systems, analysis of electromagnetic field, applied electromagnetics, intelligent electricity technology, and so on.

Dr. Huang is an Editor of the journal *Transactions of China Electrotechnical Society* and holds one PCT patent. He received the Teaching Achievement Prize of Jiang Su Province in 2009, Ministry of Environmental Protection Science and Technology Prize in 2012, and so on.

Jinpeng Guo received the B.S. degree in electrical engineering from Chongqing University, Chongqing, China, in 2014, and is currently working toward the M.S. degree in electrical engineering at Southeast University, Nanjing, China.

His research interests include designs and optimizations of wireless power transfer systems.

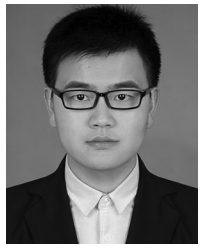

Han Liu was born in Hubei, China, in 1993. He received the B.S. degree in electrical engineering from the School of Electrical Engineering, Southeast University, Nanjing, China, in 2014, where he is currently working toward Ph.D. degree.

His research interests include wireless power transfer technology, power electronics, and electric vehicle dynamic wireless charging.

Changxin Yan received the B.S. degree in electrical engineering from Jiangsu University, Zhenjiang, China, in 2010, and is currently working toward the M.S. degree in electrical engineering at Southeast University, Nanjing, China.

Since 2014, his research interest is wireless power transfer systems.

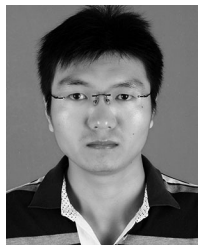

Linlin Tan received the B.S. degree in electrical engineering and automation from Harbin Engineering University, Harbin, China, in 2008, and the Ph.D. degree in electrical engineering from Southeast University, Nanjing, China, in 2014.

He is currently a Lecturer in the School of Electrical Engineering, Southeast University. He has published more than 20 papers. His research interests include wireless power transfer, wireless charging for electric vehicle, and wireless vehicle to grid.